Sean Hu for providing his linear stability analysis code for the analysis in this Note.

References

[1]Lissman, P., "Low Reynolds Number Airfoils," *Annual Review of Fluid Mechanics*, Vol. 15, 1983, pp. 223–239.

[2]Murray, J., Moes, T., Norlin, K., Bauer, J., Geenen, R., Moulton, B., and Hoang., S., "Piloted Simulation Study of a Balloon-Assisted Deployment of an Aircraft at High Altitude," NASA TM 104245, Jan. 1992.

[3]Leblanc, P., Blackwelder, R., and Liebeck., R., "A Comparison Between Boundary Layer Measurements in a Laminar Separation Bubble Flow and Linear Stability Theory Calculations," *Low Reynolds Number Aerodynamics: Proceedings of the Conference*, Springer-Verlag, New York, 1989, pp. 189–205.

[4]Dovgal, A. V., Kozlov, V. V., and Michalke, A., "Laminar Boundary Layer Separation: Instability and Associated Phenomena," *Progress of Aerospace Sciences*, Vol. 30, No. 1, 1994, pp. 61–94.

[5]McGhee, R., Walker, B., and Millard, B., "Experimental Results for the Eppler387 Airfoil at Low Reynolds Numbers in the Langley Low-Turbulence Pressure Tunnel," NASA TM4062, Oct. 1988.

[6]Drela, M., and Giles, M., "Viscous-Inviscid Analysis of Transonic and Low Reynolds Number Airfoils," *AIAA Journal*, Vol. 25, No. 10, 1987, pp. 1347–1355.

[7]Lin, J. M., and Pauley, L. L., "Low-Reynolds-Number Separation on an Airfoil," *AIAA Journal*, Vol. 34, No. 8, 1996, pp. 1570–1577.

[8]Drela, M., "Transonic Low-Reynolds-Number Airfoils," *Journal of Aircraft*, Vol. 29, No. 6, 1992, pp. 1106–1113.

[9]MacCormack, R., "Current Status of Numerical Solution of the Navier Stokes Equations," AIAA Paper 85-0032, Jan. 1985.

[10]Tatineni, M., and Zhong, X., "Numerical Simulation of Unsteady Low-Reynolds-Number Separated Flows over Airfoils," AIAA Paper 97-1929, June–July 1997.

D. S. McRae
Associate Editor

Improved Low-Reynolds-Number k–$\tilde{\epsilon}$ Model

M. M. Rahman* and T. Siikonen†
Helsinki University of Technology, FIN-02015 TKK, Finland

Introduction

THE significance of the linear eddy viscosity k–ϵ model is diminishing due to the deficiency that it cannot accurately predict nonequilibrium flows such as flows with separation and reattachment. The reasoning is most likely to be attributed to the overestimation of k. However, the inclusion of a cross-diffusion term in the ϵ equation may improve the prediction capability of the k–ϵ model, as is experienced by Yoon and Chung[1] for a compression ram flow.

An extension ascribed to the low-Reynolds-number k–$\tilde{\epsilon}$ model of Chien[2] is proposed herein. Essential modifications made in the original Chien (OCH) model include the introduction of the Taylor microscale in the eddy viscosity damping function f_μ and the additional cross-diffusion terms in the k and $\tilde{\epsilon}$ equations, which provoke the level of energy dissipation in nonequilibrium flow regions. The y^+ dependence of the damping function associated with the term that yields a quadratic growth of $\tilde{\epsilon}$ with the wall distance is eliminated by $R_y = \sqrt{(k)}\, y/\nu$. The function multiplying the constant $C_{\epsilon 2}$, which takes the free turbulence into account, is dropped out. Furthermore, the wall singularity is removed by using a physically appropriate timescale that never falls below the Kolmogorov timescale $\sqrt{(\nu/\epsilon)}$.

Received 12 October 1998; revision received 29 February 2000; accepted for publication 2 March 2000.

*Research Scientist, Department of Mechanical Engineering, Laboratory of Applied Thermodynamics, Sähkömiehentie 4.

†Professor, Department of Mechanical Engineering, Laboratory of Applied Thermodynamics, Sähkömiehentie 4.

In essence, comparisons of the model predictions with the experimental and direct numerical simulation (DNS) data for well-studied flows demonstrate that the modified Chien (MCH) model induces a significant improvement over the OCH model.

MCH Model

The proposed model determines the turbulence kinetic energy k and its dissipation rate $\tilde{\epsilon}$ by the following transport equations:

$$\frac{\partial \rho k}{\partial t} + \frac{\partial \rho U_j k}{\partial x_j} = \frac{\partial}{\partial x_j}\left(\left(\mu + \frac{\mu_T}{\sigma_k}\right)\frac{\partial k}{\partial x_j}\right) + \rho P - \rho\epsilon + E_k \tag{1}$$

$$\frac{\partial \rho \tilde{\epsilon}}{\partial t} + \frac{\partial \rho U_j \tilde{\epsilon}}{\partial x_j} = \frac{\partial}{\partial x_j}\left(\left(\mu + \frac{\mu_T}{\sigma_\epsilon}\right)\frac{\partial \tilde{\epsilon}}{\partial x_j}\right) + \left(C_{\epsilon 1}\rho P - C_{\epsilon 2}\rho\tilde{\epsilon} - \rho D e^{-(R_y/80)^2}\right)\Big|\ T_t + E_\epsilon \tag{2}$$

where $\epsilon = \tilde{\epsilon} + D$ and the turbulent production term $P = -\overline{u_i u_j}(\partial u_i/\partial x_j)$. The eddy viscosity and other variables are evaluated as

$$\mu_T = C_\mu f_\mu \rho k T_t, \qquad T_t = \max\left(k/\tilde{\epsilon}, C_T\sqrt{\nu/\epsilon}\right)$$

$$D = 2\nu k\Big|\ y_n^2, \qquad R_y = \sqrt{k}\, y_n/\nu \tag{3}$$

where y_n is the normal distance from the wall and ν represents the kinematic viscosity. The turbulence timescale T_t prevents the singularity at $y_n = 0$ in the dissipation equation. The associated constants are $C_\mu = 0.09$, $C_{\epsilon 1} = 1.44$, $C_{\epsilon 2} = 1.92$, $C_T = \sqrt{2}$, $\sigma_k = 1.0$, and $\sigma_\epsilon = 1.3$.

The near-wall damping function f_μ is taken to be a function of R_λ, defined by

$$f_\mu = 1 - \exp\left(-0.01R_\lambda - 0.0068R_\lambda^3\right)$$

$$R_\lambda = y_n\Big|\ \sqrt{\nu k/\tilde{\epsilon}} = y_n\Big|\ \sqrt{\nu T_t} \tag{4}$$

where $\sqrt{(\nu T_t)}$ is the Taylor microscale. By an analysis of the distinct effects of low Reynolds number and wall proximity, a similar type of eddy viscosity damping function is proposed by Hwang and Lin[3] in their k–$\tilde{\epsilon}$ model. The use of R_λ confronts the singularity at neither the separating nor the reattaching point, in contrast to the adoption of $y^+ = u_\tau y/\nu$, where u_τ is the friction velocity. Consequently, the model is applicable to separated and reattaching flows. In principle, Eq. (4) confirms that the Taylor microscale can be used as an estimate of the near-wall turbulence resolution, physically required to damp out the eddy viscosity.

The extra quantities E_k and E_ϵ in Eqs. (1) and (2) originate from the most extensive turbulent diffusion models for k and ϵ equations derived by Yoshizawa[4] with the two-scale direct-interaction approach using the inertial-range simplification. In the present work, a truncated version is utilized that may be provided with

$$E_k = C_k C_\mu \frac{\partial}{\partial x_j}\left(\frac{k^3}{\tilde{\epsilon}^2}\frac{\partial \tilde{\epsilon}}{\partial x_j}\right), \qquad E_\epsilon = C_\epsilon C_\mu \frac{\partial}{\partial x_j}\left(k\frac{\partial k}{\partial x_j}\right) \tag{5}$$

where C_k and C_ϵ are readjustable model constants. Actually, Eq. (5) signifies the cross-diffusion effects from $\tilde{\epsilon}$ and k in the k and $\tilde{\epsilon}$ equations, respectively. The existence of the cross-diffusion effect from the statistical viewpoint is also pointed out by Leslie.[5] Nevertheless, the contrivance herein is to model Eq. (5) so that optimal results are achievable compared with DNS and experimental data. To receive positive benefits from the numerical reliability and to integrate the condition of inertial-range simplification directly to the solid wall, the cross-diffusion terms are designed as

$$E_k = C_k \mu_T \min\left(\frac{\partial(k/\epsilon)}{\partial x_j}\frac{\partial \tilde{\epsilon}}{\partial x_j}, 0\right), \qquad E_\epsilon = C_\epsilon \frac{\mu_T}{T_t^2}\left(\frac{\partial(k/\epsilon)}{\partial x_j}\frac{\partial k}{\partial x_j}\right) \tag{6}$$

where the constants $C_k = 0.5$ and $C_\epsilon = -2C_k$ are tuned to match well-acquainted flows considered hereinafter. Obviously, both E_k and E_ϵ stimulate the energy dissipation in nonequilibrium flows, thereby reducing the departure of the turbulent length scale from its local equilibrium value.

Computations

To ascertain the efficacy of the proposed model, a few applications to two-dimensional turbulent flows consisting of a fully developed channel flow, a backward-facing step flow, and an asymmetric plane diffuser flow are considered. For a comparison purpose, calculations from the OCH model are also included. A cell-centered finite volume scheme combined with an artificial compressibility approach[6] is employed to solve the flow equations.

Channel Flow

The computation is carried out for a fully developed turbulent channel flow at $Re_\tau = 180$ for which turbulence quantities are attainable from the DNS data.[7] Calculations are conducted in the half-width of the channel, imposing cyclic boundary conditions except for the pressure. The length of the computational domain is 32δ, where δ is the channel half-width. Two different grid resolutions are provided for the MCH model to show the grid convergence. Comparisons are made by plotting the results in wall units. The results shown in Fig. 1 indicate that the MCH model predictions are qualitatively good relative to those of the OCH model.

Backward-Facing Step Flow

To validate the performance in complex separated and reattaching turbulent flows, the MCH model is applied to the flow over a backward-facing step. The computation is conducted corresponding to the experimental case with zero deflection of the wall opposite to the step, as investigated by Driver and Seegmiller.[8] The ratio between the channel height and the step height h is 9, and the step height Reynolds number is $Re = 3.75 \times 10^4$. At the channel inlet, the Reynolds number based on the momentum thickness is $Re_\theta = 5.0 \times 10^4$. A 128×128 nonuniform grid is used for the computations, and the first near-wall grid node is at $y^+ < 1.5$. The inlet profiles for all dependent variables are generated by solving the models at the appropriate momentum thickness Reynolds number.

Computed and experimental friction coefficients C_f along the bottom wall (step side wall) are plotted in Fig. 2. The distance x/h is measured exactly from the step corner. As is observed, the OCH model gives the C_f distribution with a large overshoot followed by a sudden drop in the immediate vicinity of the reattachment point. The MCH model is in surprisingly good agreement with the data. The positive C_f that starts from $x/h = 0$, is due to a secondary eddy, which sits in the corner at the base of the step, inside the main recirculation region.

Asymmetric Plane Diffuser Flow

To further evaluate the performance, the model is applied to simulate the flow in a plane asymmetric diffuser with an opening angle of 10 deg, for which measurements are available.[9] The expansion ratio of 4.7 is sufficient to produce a separation bubble on the deflected wall. Hence the configuration provides a test case for smooth, adverse-pressure-driven separation. The entrance to the diffuser consists of a plane channel to invoke fully developed flow with $Re = 2.0 \times 10^4$ based on the centerline velocity and the channel height.

Computations involving a 120×72 nonuniform grid resolution are considered to be accurate to describe the flow characteristics. The length of the computational domain is $76h$, where h is the inlet channel height. The thickness of the first cell remains below one in y^+ units on both the deflected and flat walls. Figure 3 portrays the

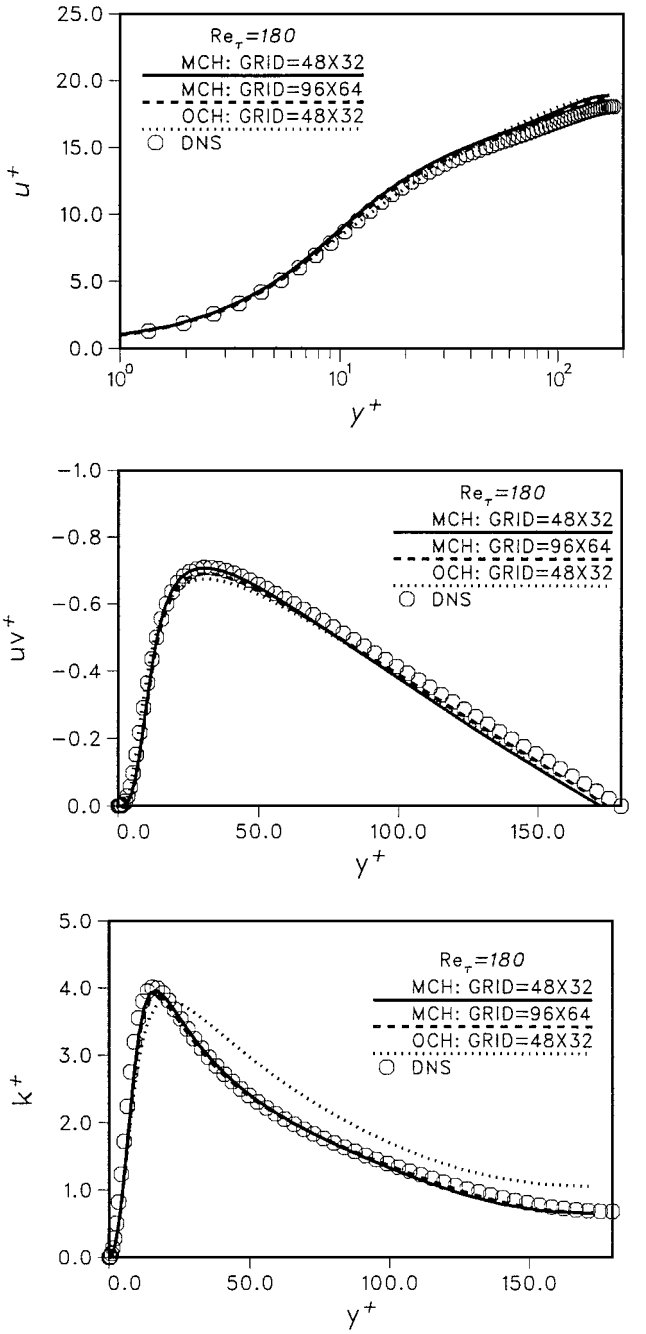

Fig. 1 Channel flow predictions compared with DNS results.

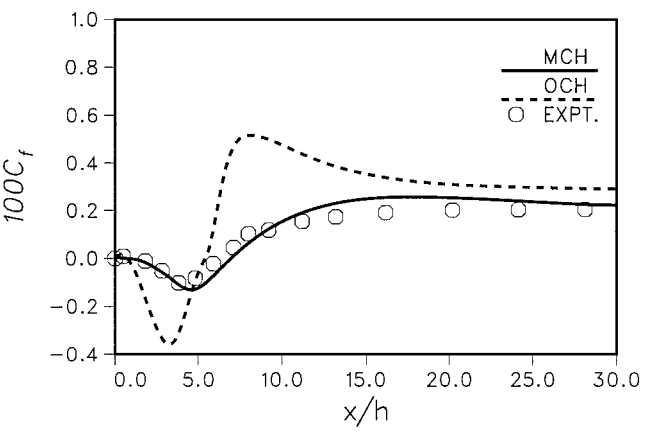

Fig. 2 Skin-friction coefficient along the bottom wall of the step flow.

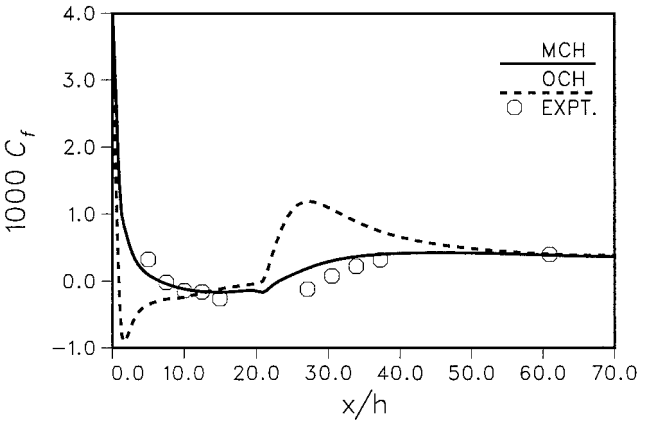

Fig. 3 Skin-friction coefficient of the diffuser flow along the deflected bottom wall.

predicted skin-friction coefficients C_f. The superior performance of the MCH model, in strong contrast to that of the OCH model, is once more ascertained. Apparently, the ambiguous prediction regarding the OCH model is attributable to shortcomings in the y^+ dependence viscous damping functions employed.

Conclusion

The potential importance of the cross diffusion together with the viscous damping functions is conspicuous. The modification introduced with the Chien model is profoundly convenient because it circumvents the defect entangled with the model to a greater extent. The MCH model accounts for the near-wall and low-Reynolds-number effects emanating from the physical requirements.

Acknowledgments

The assistance of Patrik Rautaheimo, Esa Salminen, and Petri Majander of Helsinki University of Technology, Finland, is gratefully acknowledged.

References

[1]Yoon, B. K., and Chung, M. K., "Computation of Compression Ramp Flow with a Cross-Diffusion Modified k–ϵ Model," *AIAA Journal*, Vol. 33, No. 8, 1995, pp. 1518–1521.

[2]Chien, K.-Y., "Predictions of Channel and Boundary Layer Flows with a Low-Reynolds Number Turbulence Model," *AIAA Journal*, Vol. 20, No. 1, 1982, pp. 33–38.

[3]Hwang, C. B., and Lin, C. A., "Improved Low-Reynolds-Number k–ϵ Model Based on Direct Numerical Simulation Data," *AIAA Journal*, Vol. 36, No. 1, 1998, pp. 38–43.

[4]Yoshizawa, A., "Statistical Modeling of a Transport Equation for the Kinetic Energy Dissipation Rate," *Physics of Fluids A*, Vol. 30, No. 3, 1987, pp. 628–631.

[5]Leslie, D. C., *Development in the Theory of Turbulence*, Clarendon, Oxford, 1973, pp. 335–342.

[6]Rahman, M. M., Rautaheimo, P., and Siikonen, T., "Numerical Study of Turbulent Heat Transfer from a Confined Impinging Jet Using a Pseudo-Compressibility Method," *2nd International Symposium on Turbulence, Heat and Mass Transfer*, Delft Univ. Press, Delft, The Netherlands, 1997, pp. 511–520.

[7]Mansour, N. N., Kim, J., and Moin, P., "Reynolds-Stress and Dissipation-Rate Budgets in a Turbulent Channel Flow," *Journal of Fluid Mechanics*, Vol. 194, 1988, pp. 15–44.

[8]Driver, D. M., and Seegmiller, H. L., "Features of a Reattaching Turbulent Shear Layer in Divergent Channel Flow," *AIAA Journal*, Vol. 23, No. 2, 1985, pp. 163–171.

[9]Buice, C. U., and Eaton, J. K., "Experimental Investigation of Flow Through an Asymmetric Plane Diffuser," Dept. of Mechanical Engineering, Thermosciences Div., Rept. TSD-107, Stanford Univ., Stanford, CA, 1997.

R. M. C. So
Associate Editor

Vibration of Thermally Stressed Composite Plates with and Without Cutouts

Lazarus Teneketzis Tenek*
Aristotle University of Thessaloniki, 540 06 Thessaloniki, Greece

I. Introduction

STRUCTURES made of composite materials often operate at elevated temperatures. At these temperatures thermomechanical stressing may occur. Composite structures that are thermally stressed can resonate at various frequencies. It is therefore of interest to examine the vibration behavior of structures made of composite materials that are thermally stressed. Of particular interest is the effect of initial thermal stressing to the subsequent oscillating behavior of composite panels. The present study considers two laminated composite plates; an eight-layer $(0/90/0/90)_s$ cross-ply laminate and an eight-layer quasi-isotropic $(45/-45/0/90)_s$ composite plate. Both plates are thermally stressed via the application of various temperatures. Following thermal stressing, an eigenvalue problem is considered, and the first natural frequency of the structure is extracted.

Researchers have started to study the vibration behavior of composite structures at elevated temperatures.[1–5] The frequency-temperature curves are nonlinear in nature and are affected by the particular lamination. The present study considers the effect of the temperature on the fundamental natural frequency of laminated composite plates with and without cutouts. The effect of thermal stressing on the fundamental frequency of composite plates with holes is compared with the corresponding effect of laminates without cutouts.

II. Computational Experiments

Figure 1 shows a laminated composite plate along with all geometrical and material properties. The left edge of the plate cannot move in the three directions, whereas in all other edges the vertical displacement is prohibited. Uniform temperature increase is applied on the top and bottom boundaries. A small central cutout is considered as depicted in the figure. Two eight-layer laminations are considered, namely cross-ply $(0/90/0/90)_s$ and quasi-isotropic $(45/-45/0/90)_s$. The application of temperature introduces the geometrically nonlinear problem

$$K_T r = J \tag{1}$$

where K_T is the tangent stiffness and J is the initial load caused by temperature. The temperature is applied incrementally, and following convergence and the full application of the incremental temperature the following eigenvalue problem is solved:

$$K_T x = \lambda M x \tag{2}$$

where M is the global mass matrix, λ the eigenvalue (natural frequency), and x the eigenvector.

The composite plate is discretized with a set of triangular elements based on the natural-mode finite element method.[6] In brief, the triangular finite element is assigned a set of rigid-body and straining modes. The latter are equal to the global nodal degrees of freedom minus the number of rigid-body modes.

Figure 2 shows the temperature-frequency curves for an eight-layer $(0/90/0/90)_s$ cross-ply laminate with and without cutouts. We observe that from $T = 0$ to 120°C the presence of the cutout results in a decrease of the natural frequency of the plate. At subsequent frequencies however, the natural frequency of the plate with the cutout

Received 14 February 2000; accepted for publication 11 March 2000.

*Senior Research Scientist, Laboratory of Mechanics and Materials, Polytechnic School, Box 468.